

## EFFECT OF JUNCTION GEOMETRY ON ACOUSTIC RESPONSE OF SIDE BRANCH RESONATORS

A. Velikorodny, T. Yan, P. Oshkai  
*University of Victoria, Victoria, BC, Canada*

### ABSTRACT

*Flow-acoustic coupling due to turbulent flow over coaxial deep cavities (side branches) mounted in a duct is investigated using digital particle image velocimetry (PIV) and unsteady pressure measurements.*

*Structure of the acoustic noise source is characterized in terms of patterns of generated acoustic power. A semi-empirical approach that involves numerical calculation of the acoustic (irrotational) velocity and experimental measurements of total velocity is employed for acoustic power calculation.*

*In addition to the basic side branch configuration, effect splitter plates placed in the junction region is characterized in terms of acoustic response of the system as well as quantitative flow patterns.*

*The acoustic noise source structure is strongly dependent on the degree of separated shear layer interaction. As the amplitude of the transverse flow oscillations increases, circulation of the large-scale vortical structures rapidly grows, and the region of the acoustic power production shifts upstream. In addition, Strouhal mode of the separated shear layer oscillations also has a significant effect on spatial structure and strength of the acoustic source.*

### 1. INTRODUCTION

The flow acoustic coupling phenomena is encountered in many industrial processes involving transport of the fluid through a pipeline. Resonance occurs when there is a coupling between the self-sustained oscillations of the separated shear layers and acoustic modes of the side branch. In this scenario, several authors including Chen and Sturchler (1977) and Baldwin and Simmons (1986) reported high-amplitude pressure pulsations and flow oscillations

High-amplitude pressure fluctuations, which are characteristics of the flow-acoustic coupling in the side branch systems, have been a subject of many investigations, as summarized by Ziada and Bühlmann (1992). Rockwell and Naudascher (1978) provided classification of various fluid-resonant oscillators, including side branch resonators. Keller and Escudier (1983) investigated flow-acoustic resonances in cavities for high Mach numbers. It

was shown that the excitation mechanism is gas dynamic in nature. In contrast to the edge-tone generation mechanism (i.e. impingement of vortical structures on a solid boundary), which is predominant in the case of low Mach number flows. Shear layers that form between the moving fluid in the main duct and the stationary fluid in the side branch exhibit a hydrodynamic instability. When the frequency of the hydrodynamic instability matches the resonant acoustic mode of the side branch, energy is transferred from the acoustic field, which results in formation of large-scale vortical structures that are convected across the mouth of the cavity. Subsequent deceleration of these vortices due to their interaction with the downstream corner of the cavity results in transfer of the energy of the fluctuating shear layer to the acoustic field. This resonance contributes to the increase of the amplitude of the acoustic waves.

Identification of the shape of the acoustic noise source and the contribution of individual vortices to the generated acoustic power presents significant challenges despite considerable insight that has been provided by a number of recent investigations. Hourigan et al. (1986) and Stoneman et al. (1988) characterized acoustically-coupled shear layer oscillations in terms of the number of vortices formed in the shear layer during a typical oscillation cycle. The theoretical framework for these experimental and numerical studies was provided by Howe (1975). In addition, Dequand et al. (2003a) studied behaviour of acoustically-coupled flows over cavity resonators, identifying characteristic flow regimes and providing numerical and analytical models of the flow. More recently, flow-acoustic coupling phenomenon for cavity flows was investigated by Amandolese et al. (2004), Oshkai and Yan (2006), and Arthurs et al. (2006).

The present study focuses on a coaxial side branch system, which involves two side branches mounted on the opposite sides of a rectangular duct and inline with each other. A schematic of the experimental arrangement is shown in Fig. 1. Splitter plates of various lengths were deployed along the centerline of the cross-junction, as it is shown in Fig. 2.

The splitter plates are used in industry for various purposes. Howe (1986) theoretically studied the effect of the perforated screens in dissipation of

sound in large industrial heat exchangers. Recently, Arthurs et al. (2006) investigated the effect of a splitter plate that spans across the entire side branch in order to limit propagation of the acoustic waves.

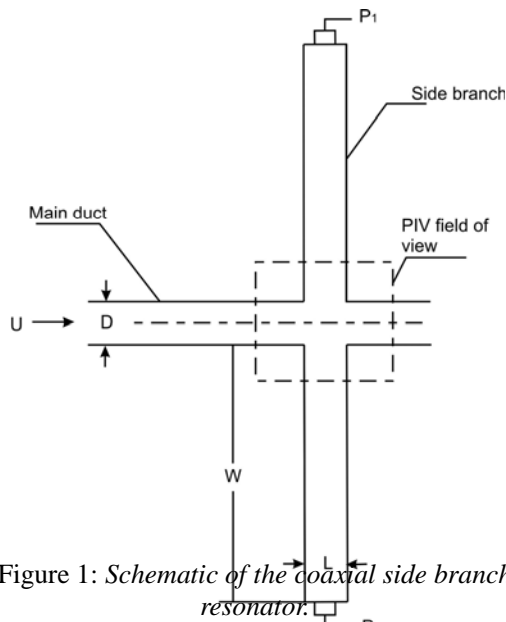


Figure 1: Schematic of the coaxial side branch resonator.

In the present study, global, quantitative images of the flow were obtained using digital particle velocimetry (DPIV). These experimental data in conjunction with measurements of acoustic pressure provide insight into the location of the acoustic source corresponding to two distinct hydrodynamic modes of shear layer oscillation. The acoustic velocity was deduced from the numerically calculated 2D velocity potential. Combination of the calculated acoustic velocity with the experimentally-obtained velocity resulted in a semi-empirical model for acoustic power calculation, outlined in Section 5.

The effect of the splitter plates on the acoustic response of the resonator is described in Section 3. In contrast to the experiments of Arthurs et al. (2006), the plates in the present study did not span across the entire side branch, which limited their interference with the acoustic wave propagation.

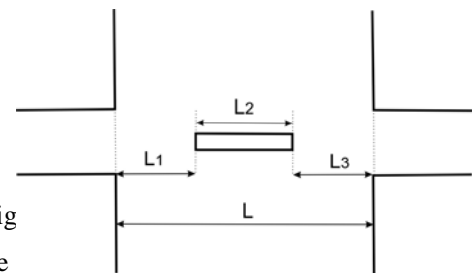
## 2. EXPERIMENTAL SYSTEM AND TECHNIQUES

Complete details of the experimental system are described by Oshkai and Yan (2006). Only the essential features are described herein. Schematic of the experimental apparatus is shown in Figure 1.

Air was supplied by a compressor located in a separate room and isolated from the experimental

apparatus. The main duct, and the coaxial side branch arrangement, allowed variations of the channel geometry, and optical access to the separated flow area(s). The duct had a streamwise length of 492 mm and a height (the out-of-page dimension) of 25.4 mm. Two coaxial side branches were mounted on the opposite sides of the main duct, 454 mm downstream of the duct inlet. The side branches had a square cross-section, and were constructed of a 3.2 mm-thick aluminum. The main duct extended for additional 12.6 mm downstream of the side branch arrangement.

In order to limit the hydrodynamic interaction of the shear layers and potentially alleviate the intensity of acoustic resonances a splitter plate was placed in the middle of the cross-junction (Fig. 2). In the present investigation, the flow features are compared for three cases corresponding to different lengths of the splitter plate. These cases are corresponding to  $L_2 = 0$  (no splitter plate), 5, and 10 mm.



Fig

Figure

microphone pressure transducers ( $P_1$  and  $P_2$ ) that were used to measure unsteady pressure in the system. The pressure transducers had a nominal sensitivity of 10340 V/Pa and were deployed at the dead ends of side branch resonator. The pressure signals were converted to a digital form at the time of acquisition.

Digital particle image velocimetry (DPIV) was employed to obtain global, quantitative flow images. Oil droplets with the typical diameter of approximately  $1 \mu\text{m}$  were used as tracer particles. Flow area indicated in Fig. 1 by a dashed rectangle was illuminated by a pulsed laser sheet. Images of the tracers were captured by a high-resolution digital camera and processed to yield global instantaneous flow velocity measurements. Depending on the flow velocity and the factor of magnification of the camera lens, the delay between the two pulses was adjusted in order to obtain adequate displacements of the particle images on the Complementary Metal Oxide Semiconductor (CMOS) sensor while providing sufficiently high spatial resolution of the flow features.

For the present study, a lens with a focal length of 60 mm was used in conjunction with a 1024 x 1024 pixel CMOS sensor to provide a physical resolution of 30 pixels/mm, which corresponds to the velocity vector field resolution of 0.35 x 0.35 mm. The system could provide up to 1500 cross-correlated images per second.

The trigger signal to the laser was recorded together with the acoustic pressure signals. This provided the information regarding the phase of acquisition of each velocity field with respect to a typical acoustic cycle, and was used for phase-averaged velocity calculation.

### 3. OVERVIEW OF ACOUSTIC RESPONSE

The measured frequency and the pressure amplitude for the configuration without the splitter plate are plotted in Fig. 3 as functions of the flow velocity in the main duct. The data points shown in the plot correspond to the points of maximum pressure amplitude at each velocity value.

It is observed that when the flow tone is generated, it is not associated with a single value of velocity, but rather with a range of velocities. There exists a minimum threshold velocity, which is required to excite the resonance. The resonance is observed to occur over three ranges of flow velocity. The frequency of the dominant resonant mode switches from the first to the fifth acoustic mode as the flow velocity  $U$  reaches approximately 31 m/s. Subsequently, the dominant frequency switches to the third mode at 39 m/s, and then to seventh acoustic and second hydrodynamic mode at 43 m/s. The maximum resonance amplitude is approximately 120 dB.

The following formula that is based on linear stability analysis, was used to calculate frequencies of hydrodynamic (Strouhal) modes of the shear layer oscillation.

$$f = \frac{U_c}{U} \left( n_s - \frac{1}{4} \right) \left( \frac{U}{L_{eff}} \right), \quad (1)$$

where  $f$  is the shear layer oscillation frequency,  $U$  is the mean flow velocity,  $U_c$  is the convective speed of the vortices,  $n_s$  is the hydrodynamic (Strouhal) mode number that indicates the number of vortices formed in the shear layer during a typical oscillation period, and  $L_{eff}$  is effective length of the cavity.

Measurements of the frequencies of the flow tones have been performed for a variety of external boundary layer flows (Blake, 1986). For small values of  $\delta/L$ , where  $\delta$  is the boundary layer thickness, the reported Strouhal numbers suggest relatively high values of average vorticity

convection velocity. More specifically,  $U_c/U$  varies from 0.33 to 0.61. In the present investigation a value of  $U_c/U$  of 0.45 was used in the calculation of the hydrodynamic frequencies.

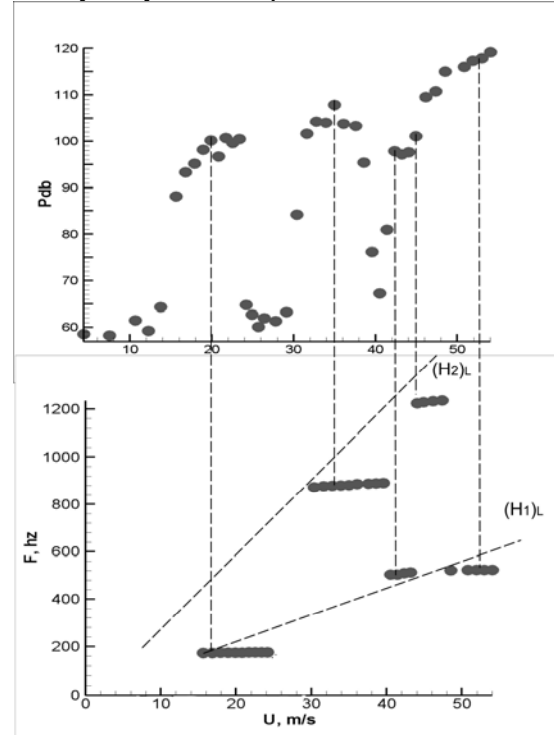


Figure 3: Pressure amplitude and frequency as functions of incoming velocity ( $L_2=0$  mm).

The diagonal lines labeled as  $(H_1)_L$  and  $(H_2)_L$  in Fig. 3 correspond to the calculated first and second hydrodynamic (Strouhal) modes, with  $L$  (cavity length) being the characteristic length. The first calculated hydrodynamic mode ( $(H_1)_L$ ) provides a good fit to the measured frequencies, while second mode ( $(H_2)_L$ ) over-predicts the experimental data. This discrepancy is due to a more complex interaction between vortices in the separated turbulent shear layer that is a characteristic of the second hydrodynamic oscillation mode.

Considering the response of the resonator in the presence of a 5 mm-long splitter plate (Fig. 4), it can be observed that only the first hydrodynamic oscillation mode results in tone generation. When a splitter plate is present in the cross-junction region, the maximum pressure amplitude decreases to 115 dB. Frequencies of the hydrodynamic shear layer oscillation modes (Strouhal modes) as functions of flow velocity were calculated using Eqn. (1) several values of effective cavity length ( $L_{eff} = L_1, L_2,$  and  $L_3$ , as they are defined in Fig. 2). It should be noted that the experimental data corresponds to the

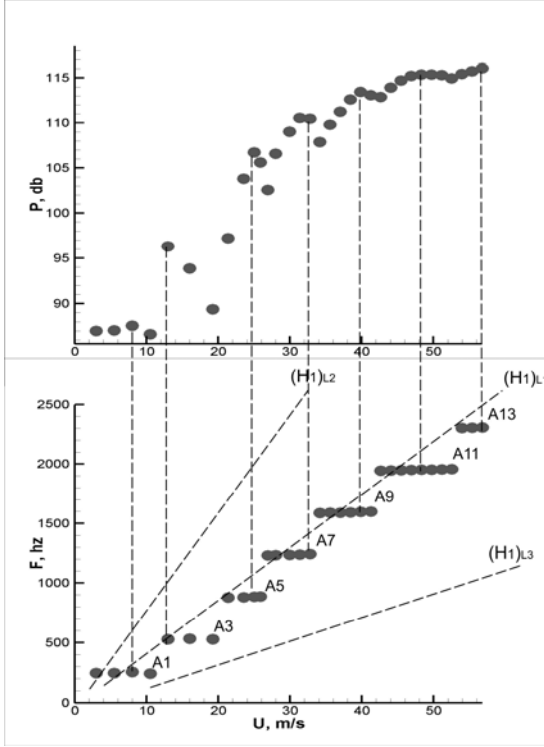


Figure 4: Pressure amplitude and frequency as functions of incoming velocity ( $L_2 = 5\text{mm}$ )

hydrodynamic mode that is based on  $L_{eff} = L_1$  ( $(H_1)_{L_2}$ ), while hydrodynamic modes that were calculated using the values of  $L_{eff} = L_2$  and  $L_{eff} = L_3$  ( $(H_1)_{L_2}$  and  $(H_1)_{L_3}$ ) respectively over- and under-predict the experimental data.

In the case of a 10 mm-long splitter plate ( $L_2 = 10\text{ mm}$ ), the data trend remains qualitatively similar to the case of  $L_2 = 5\text{ mm}$ . The Strouhal (hydrodynamic) mode of the shear layer oscillation also corresponds to a characteristic length  $L_{eff} = L_1$  (the distance between the upstream edge of the side branch and the leading edge of the plate). The maximum pressure amplitude further decreased to 112 dB. In contrast to the case of  $L_2 = 5\text{ mm}$ , both calculated  $(H_1)_{L_2}$  and  $(H_1)_{L_3}$  modes under-predict the experimental data.

In general, for all three cases, using the distance between the upstream edge of the side branch and the leading edge of the plate ( $L_{eff} = L_1$ ) for evaluation of the hydrodynamic shear layer frequencies results in the best correspondence between the calculated Strouhal mode and the experimental data. It should also be noted that the presence of the splitter plate did not significantly affect the theoretically predicted acoustic modes of the system, while hydrodynamic features were significantly affected. Generation of vorticity around the splitter plate affects the amount of energy that is transferred between the vorticity-bearing flow and the resonant acoustic field. As a

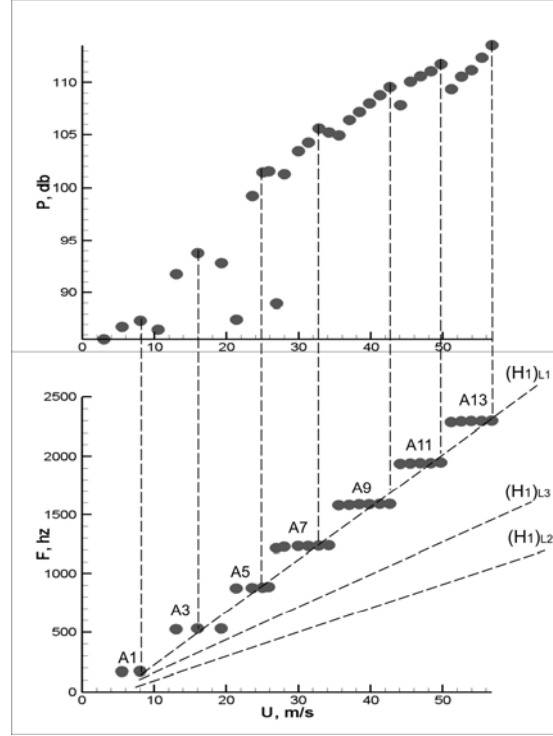


Figure 5: Pressure and frequency as functions of incoming velocity ( $L_2 = 10\text{mm}$ )

result, the maximum values of acoustic pressure decrease as the splitter plate length  $L_2$  is increased.

#### 4. INSTANTENEOUS FLOW PATTERNS

An insight into the physics of the acoustically-coupled shear layers is provided by global quantitative flow imaging using PIV. Figures 6 and 7 provide an overview of the out-of-plane vorticity distribution for the cases of  $L_2 = 0$  (no splitter plate) and  $L_2 = 5\text{ mm}$  respectively.

For both cases, the mean flow velocity is  $U = 28\text{ m/s}$  and the acoustic frequency  $f = 877\text{ Hz}$ , which yields a Strouhal number of  $Sr = fL/U = 0.79$ . The observed value of the dimensionless acoustic velocity  $U_{ac}/U$  for this case is equal to 0.0005. Assuming planar acoustic wave propagation inside the side branches, the acoustic velocity amplitude  $U_{ac}$  can be determined from the acoustic pressure amplitude  $P$ :  $U_{ac} = P / \rho_0 c_0$ , where  $\rho_0$  is the mean fluid density and  $c_0$  is the speed of sound.

The vorticity plots illustrate formation of large-scale vortical structures in the separated shear layers. As the vortices are convected downstream along the cavity opening, their peak vorticity is decreased, but the overall circulation values increase due to a larger spatial extent and higher convective speed.

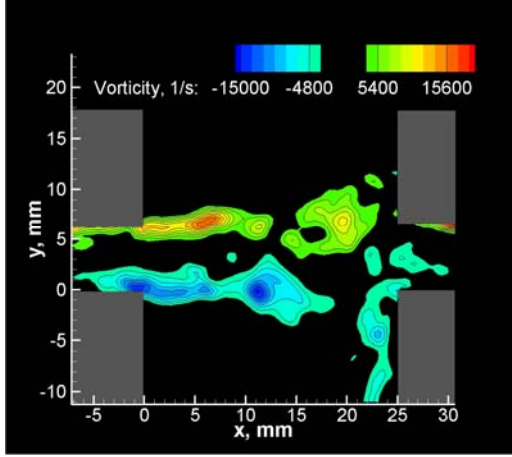


Figure 6: Pattern of instantaneous out-of-plane vorticity corresponding to the  $L_2=0$  mm case.

Images presented herein for the  $L_2 = 0$  case correspond to the second hydrodynamic mode of the shear layer oscillation, when two large-scale vortices form in the shear layer during a typical oscillation cycle.

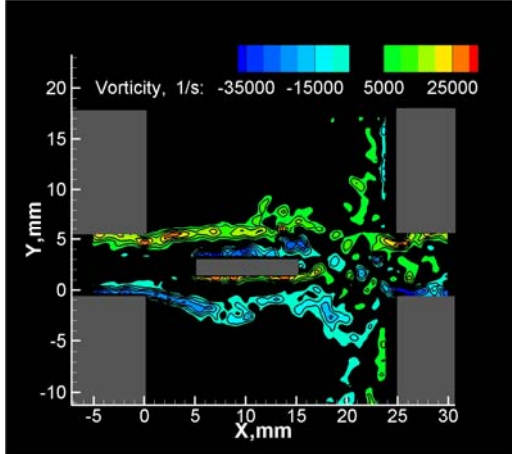


Figure 7: Pattern of instantaneous out-of-plane vorticity corresponding to the  $L_2=10$  mm case.

In contrast, the case involving the splitter plate (Fig.7) corresponds to the first hydrodynamic mode. The presence of the splitter plate significantly affects the dynamics of the shear layers along the entire span of side branches. Hydrodynamic interaction between the vortices in the upper and lower shear layers is substantially limited. Moreover, the effective length over which the shear layers can freely develop is decreased compared to the case without a splitter plate shown in Fig. 6. When the splitter plate is present, this effective development length corresponds to the distance between the upstream corners of side branches ( $x = 0$ ) and the leading edge of the splitter plate ( $x = 5$  mm and 7 mm respectively). The decrease of the distance that is available for the shear layer development results in a rapid rollup of the

separated shear layers and enhanced transverse flow oscillations in the area downstream of the separation ( $x = 0 - 10$  mm).

Flow pattern shown in Fig. 7 shows formation of boundary layers along the upper and lower surfaces of the splitter plate. The separated cavity shear layers interact with the vortices in the splitter plate boundary layers, which results in formation of a wake with a complex structure in the area between the trailing edge of the splitter plate and the downstream corners of the side branches.

## 5. ACOUSTIC POWER

The instantaneous acoustic power  $P_w$  generated by vorticity  $\underline{\omega}$ , within a volume  $V$  can be obtained from

$$P_w = \iiint_V -\rho_0 (\underline{\omega} \times \underline{V}) \cdot \underline{u}_{ac} dV, \quad (2)$$

where  $\rho_0$  is the fluid density,  $\underline{V}$  is the fluid velocity, and  $\underline{u}_{ac}$  is the acoustic particle velocity.

The theoretical framework for this approach to acoustic power calculation has been developed by Howe (1975). It should be noted that the case without a splitter plate can be represented by a jet-drive model outlined by Dequand et al. (2003a, b). The hydrodynamic contribution to the acoustic power integral,  $(\underline{\omega} \times \underline{V})$ , was calculated based on the global phase-averaged flow measurements. The amplitudes of the horizontal and vertical components of the acoustic particle velocity  $\underline{u}_{ac}$  were determined from the values of the local acceleration due to fluctuations of acoustic pressure  $p$ :

$$(U_{ac})_i = -\frac{1}{2\pi f \rho_0} \frac{\partial p}{\partial x_i}, \quad (3)$$

where  $f$  is the resonant frequency. The acoustic velocity fluctuations were assumed to be  $\pi/2$  radians out-of-phase with the fluctuations of the acoustic pressure.

Figure 8 shows spatial distribution of the integrand of Eqn. (2) for the case without splitter plates ( $L_2=0$  mm). Immediately after the separation, the amplitude of the transverse oscillations of the shear layers is limited, and two discrete source-sink pairs exist in the vicinity of the upstream corner of the junction. The two source regions with peak amplitudes of 190 N/sec are located at  $x = 4$  mm. Farther downstream, the transverse shear layer undulations increase in amplitude, and a large single source of acoustic power is present. This source region exhibits high levels of generated acoustic power due to increased circulation of the large-scale vortices. Prior to impingement on the downstream side branch corner, the two interacting shear layers produce a single large-scale sink region.

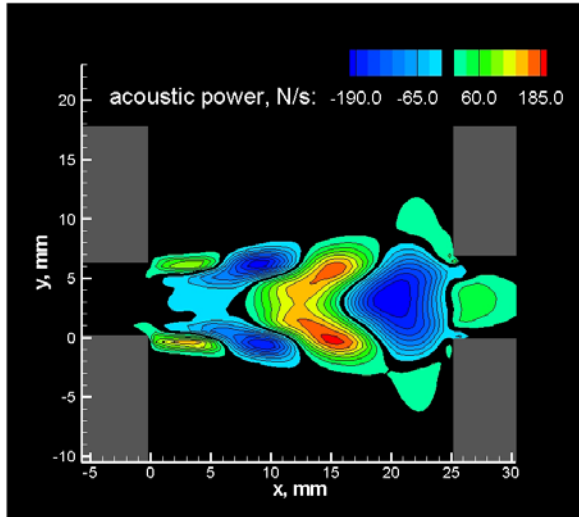


Figure 8: Patterns of time-averaged acoustic power corresponding to the second hydrodynamic oscillation mode:  $L_2=0$  mm.

It is expected that with the presence of plates in the cross-junction the maximum values of acoustic power will decrease due to interaction of the acoustic field with the vortices shed from the splitter plate. As a result, reduced amount of acoustic energy will be available for assisting in formation of large-scale vortical structures in the side branch shear layers. This phenomenon is utilized in large-scale industrial heat exchangers where perforated screens are used for sound dissipation (Howe, 1986). Current pressure response measurements illustrate this trend of acoustic response, as it is described in Section 3.

## 6. CONCLUSIONS

Acoustic response of a coaxial side branch resonator was investigated using a combination of particle image velocimetry (PIV) imaging with the measurements of unsteady acoustic pressure. Resonant flow tones corresponding to two hydrodynamic modes of shear layer oscillation are characterized in terms of acoustic pressure amplitude and frequency of the dominant pressure peaks.

The modification to the cross-junction geometry has been introduced by deploying splitter plates along the centerline of the channel. The shear layers remained coupled through the acoustic field, while the hydrodynamics was affected due to presence of splitter plates. The decrease in maximum pressure amplitudes with the increased length of the splitter plate has been observed. It is suggested that this decrease is due to interaction between the acoustic waves and the vortices generated by the splitter plate. Future work will include calculation of

acoustic power in order to quantify energy transfer between hydrodynamic and acoustic fields.

## 7. REFERENCES

- Amandolese, X., et al., 2004, An experimental study of the acoustic oscillations by flows over cavities. *Journal of Vibration and Acoustics*. **126**: p. 190-195.
- Arthurs, D., et al. *Flow Induced Acoustic Resonances of an Annular Duct with Co-Axial Side Branches* in ASME Pressure Vessels and Piping Division Conference. 2006. Vancouver, BC, Canada.
- Baldwin, R.M. and H.R. Simmons, 1986, Flow-induced vibration in safety relief valves. *ASME Journal of Pressure Vessel Technology*. **108**(3): p. 267-272.
- Blake, W.K., *Mechanics of Flow-Induced Sound and Vibration*. 1986, New York: Academic Press.
- Chen, Y.N. and R. Sturchler. *Flow-induced vibrations and noise in a pipe system with blind branches due to coupling of vortex shedding*. in *Internoise 77*. 1977. Zurich.
- Dequand, S., et al., 2003a, Self-sustained oscillations in a closed side branch system. *Journal of Sound and Vibration*. **263**: p. 359-386.
- Dequand, S., et al., 2003b, Simplified models of flue instruments: Influence of mouth geometry on the sound source. *Journal of Acoustical Society of America*. **113**: p. 1724-1735.
- Hourigan, K., et al. *Flow-induced acoustic resonance for a bluff body in a duct: a numerical study*. in *9th Australian fluid mechanics conference*. 1986. Auckland.
- Howe, M.S., 1986, Attenuation of sound due to vortex shedding from a splitter plate in a mean flow duct. *Journal of Sound and Vibration*. **105**(3): p. 385-396.
- Howe, M.S., 1975, Contributions to the theory of aerodynamic sound, with applications to excess jet noise and the theory of the flute. *Journal of Fluid Mechanics*. **71**: p. 625-673.
- Keller, J.J. and M.P. Escudier, 1983, Flow-excited resonances in covered cavities. *Journal of Sound and Vibration*. **86**(2): p. 199-226.
- Oshkai, P. and T. Yan. *Experimental Investigation of Coaxial Side Branch Resonators*. in ASME Pressure Vessels and Piping Division Conference. 2006. Vancouver.
- Rockwell, D. and E. Naudascher, 1978, Review of self-sustaining oscillations of flow past cavities. *ASME Journal of Fluids Engineering*. **100**: p. 152-165.
- Stoneman, S.A.T., et al., 1988, Resonant sound caused by flow past two plates in tandem in a duct. *Journal of Fluid Mechanics*. **192**: p. 455-484.
- Ziada, S. and E.T. Bühlmann, 1992, Self-excited resonances of two side-branches in close proximity. *Journal of Fluids and Structures*. **6**: p. 583-601.